



Article

HIV-1 Tat Upregulates the Receptor for Advanced Glycation End Products and Superoxide Dismutase-2 in the Heart of Transgenic Mice

Alaa N. Qrareya ¹, Nason S. Wise ¹, Emmanuel R. Hodges ¹, Fakhri Mahdi ¹, James A. Stewart, Jr. ^{1,2,*}
and Jason J. Paris ^{1,2,*}

¹ Department of BioMolecular Sciences, School of Pharmacy, University of Mississippi, Oxford, MS 38677, USA

² Research Institute of Pharmaceutical Sciences, University of Mississippi, Oxford, MS 38677, USA

* Correspondence: jastewa7@olemiss.edu (J.A.S.J.); parisj@olemiss.edu (J.J.P.); Tel.: +1-662-915-2309 (J.A.S.J.); +1-662-915-3096 (J.J.P.)

Abstract: Cardiovascular disorder (CVD) is a common comorbidity in people living with HIV (PLWH). Although the underlying mechanisms are unknown, virotoxic HIV proteins, such as the trans-activator of transcription (Tat), likely contribute to CVD pathogenesis. Tat expression in mouse myocardium has been found to induce cardiac dysfunction and increase markers of endothelial toxicity. However, the role that Tat may play in the development of CVD pathogenesis is unclear. The capacity for Tat to impact cardiac function was assessed using AC16 human cardiomyocyte cells and adult male and female transgenic mice that conditionally expressed Tat [Tat(+)], or did not [Tat(-)]. In AC16 cardiomyocytes, Tat increased intracellular calcium. In Tat(+) mice, Tat expression was detected in both atrial and ventricular heart tissue. Tat(+) mice demonstrated an increased expression of the receptor for advanced glycation end products and superoxide dismutase-2 (SOD-2) in ventricular tissues compared to Tat(-) controls. No changes in SOD-1 or α -smooth muscle actin were observed. Despite Tat-mediated changes at the cellular level, no changes in echocardiographic measures were detected. Tat(+) mice had a greater proportion of ventricular mast cells and collagen; however, doxycycline exposure offset the latter effect. These data suggest that Tat exposure promotes cellular changes that can precede progression to CVD.

Keywords: cardiomyocytes; echocardiography; receptor for advanced glycation end products; superoxide dismutase; trans-activator of transcription



Citation: Qrareya, A.N.; Wise, N.S.; Hodges, E.R.; Mahdi, F.; Stewart, J.A., Jr.; Paris, J.J. HIV-1 Tat Upregulates the Receptor for Advanced Glycation End Products and Superoxide Dismutase-2 in the Heart of Transgenic Mice. *Viruses* **2022**, *14*, 2191. <https://doi.org/10.3390/v14102191>

Academic Editor: Mark R. Krystal

Received: 19 August 2022

Accepted: 27 September 2022

Published: 4 October 2022

Publisher's Note: MDPI stays neutral with regard to jurisdictional claims in published maps and institutional affiliations.



Copyright: © 2022 by the authors. Licensee MDPI, Basel, Switzerland. This article is an open access article distributed under the terms and conditions of the Creative Commons Attribution (CC BY) license (<https://creativecommons.org/licenses/by/4.0/>).

1. Introduction

Advanced human immunodeficiency virus-1 (HIV-1) treatments have reduced HIV-associated morbidity and mortality [1–3]. However, people living with HIV (PLWH) are more likely to develop premature age-related comorbidities compared to age-matched healthy individuals [4–9]. As such, PLWH experience cardiovascular diseases (CVDs) such as heart failure [10,11], cardiomyopathy [12], myocardial infarction [13,14], coronary heart disease [15–17], and sudden cardiac death [18,19] in greater proportions compared to same-aged seronegative individuals. CVDs are the main leading cause of death globally [20]; however, the risk of CVDs is higher among PLWH [21], and its incidence increases with age [22,23]. The proportion of older PLWH who experience CVDs is expected to further increase (~78%) by 2030 [22]. Antiretroviral therapies cannot entirely eradicate viral proteins or promote full immune system recovery [24,25]. Therefore, persistent viral proteins may contribute to the risk of CVD in HIV.

The trans-activator of transcription (Tat) is a non-structural HIV protein secreted from infected cells, predominantly CD4⁺ T cells, as well as monocytes/macrophages, to enhance viral replication [26,27]. Tat is also found to exert deleterious effects on the myocardium. Tat induces endothelial cell dysfunction, including vasculopathy via the

increased expression of vascular cell adhesion molecule-1 [28]; activation of monocyte recruitment and adhesion [29]; and endothelial senescence, mediated in part by microRNA-34 signaling in cultured endothelial cells [30]. Moreover, Tat exerts vascular and atherogenic effects mediated by the NF- κ B pathway [29,31–33]. In addition to these structural changes, Tat alters mitochondrial function and exacerbates the production of reactive oxygen species (ROS) in cultured cardiomyocytes [34]. Furthermore, Tat induces bradycardia by activating parasympathetic neurons within the nucleus ambiguus [35] and mediates vascular aging in rodents [30]. Although the Tat-mediated mechanisms that may contribute to CVDs are not well understood, Tat has been demonstrated to upregulate the receptor for advanced glycation end products (RAGE) within the blood-brain barrier [36–38], a receptor target known to be involved in CVD [39,40].

Advanced glycation end products (AGEs) are non-enzymatic glycation and oxidation products crosslinked to proteins, lipids, and nucleic acids [41]. The accumulation of AGEs increases the risk of CVD by binding to their receptor, RAGE [42]. AGE-RAGE signaling is involved in neointimal hyperplasia formation after vascular injury [43], the exacerbation of ROS production [44,45], the alteration of endothelial function [44], and the attenuation of cardiac fibroblast migration [46]. The formation of endogenous AGEs is accelerated during inflammation, aging, and oxidative stress [41]. As such, levels of circulating AGEs are elevated in PLWH [47,48], concurrent with greater levels of oxidative stress, pro-inflammation [47], and disease-related cardiometabolic biomarkers compared to seronegative people [48]. Furthermore, the levels of soluble RAGE in the serum of PLWH were positively correlated with carotid atherosclerosis [49]. However, the impact of Tat on AGE-RAGE signaling in the myocardium needs to be investigated. Herein, we examined the impact of HIV-1 Tat exposure on the development of cardiovascular abnormalities in adult (2–6 months old) HIV Tat-transgenic mice. We hypothesized that conditional Tat expression would increase the expression of RAGE within the heart concurrent with the cardiac abnormalities.

2. Materials and Methods

All experimental procedures were preapproved by the Institutional Animal Care and Use Committee at the University of Mississippi and conducted in accordance with the National Institutes of Health Guide for Care and Use of Laboratory Animals (NIH Publication No. 85-23) ethical guidelines.

2.1. Intracellular Calcium Imaging

The human cardiomyocyte AC16 cell line was obtained from Millipore Sigma (#SCC109). Cells were cultured in Dulbecco's modified Eagle's medium: nutrient mixture F-12 (DMEM/F-12) containing 2 mM L-glutamine, 12.5% FBS, and 1 \times penicillin-streptomycin. Cardiomyocytes were seeded (3×10^3 cells/dish) on 35 mm glass-bottom Petri dishes. For calcium measurement, Fluo-4 AM (5 μ M) was used and prepared per manufacture instructions (catalog #F10489, Thermo Fisher, Waltham, MA, USA). Cells were loaded with Fluo-4 AM for 30 min prior to Tat treatment. Loaded-cells were incubated at 37 $^{\circ}$ C for 20 min, then 15 min at room temperature. After incubation, cells were washed twice with Hank's balanced salt solution. Time-lapse fluorescent microscopy was conducted using an inverted Nikon Ti2E microscope (ex/em: 494 nm/506 nm) over 10 min (1 image/second for the first 2 min; 1 image/30 s for the next 8 min; [50]). Cells were stimulated either with Tat (50 ng/mL: ImmunoDx, Woburn, MA, USA) or water after 30 s of starting live-cell imaging. Images were acquired and analyzed using NIS-analysis software (Nikon, Melville, NY, USA). Four microscopic fields were assessed in each dish. Within each field, fluorescent intensity was assessed for every cell in the field. For each cell, the mean of four randomly selected regions of interest (ROIs) on the soma was measured. Differences in fluorescent intensity from baseline were calculated for each culture using the following formula: $f - f_0/f_0$.

2.2. Animal and Housing

Adult (2–6 months old) male ($n_{\text{Tat}(-)} = 48$, $n_{\text{Tat}(+)} = 63$), and female ($n_{\text{Tat}(-)} = 25$, $n_{\text{Tat}(+)} = 21$) HIV-1 Tat transgenic mice were generated in the vivarium at the University of Mississippi (University, MS, USA). Mice were housed (3–5/cage) on a reversed 12:12 h light-dark cycle (lights off at 09:00 h) in a temperature/humidity-controlled environment.

2.3. HIV-1 Tat Induction

HIV-1 Tat protein was conditionally expressed via the administration of doxycycline (Dox) hyclate (56 mg/kg; Cayman Chemical, Ann Arbor, MI, USA), as previously described [51]. Briefly, Tat(+) mice express the *tat* transgene and a reverse tetracycline-controlled transactivating (rtTA) transcription factor, whereas Tat(−) mice express only the rtTA transcription factor [51]. In this mouse model, *tat* expression is driven by a GFAP-relegated promoter. While the majority of GFAP⁺ cells reside in the central nervous system [52,53], there is known GFAP expression in the heart, as well [54–56].

To induce Tat exposure, Tat(+) and Tat(−) mice received intraperitoneal injections of Dox over 5 consecutive days, followed by 2–21 days of Dox wash-out in order to avoid nonspecific effects of Dox (Dox $t_{1/2} = 5–6$ h; [57]). As an additional control, some Tat-transgenic mice received saline injections and were included as uninduced negative controls.

2.4. Echocardiography

All mice underwent a transthoracic echocardiography protocol using VEVO 3100 Ultrasound system (FUJIFILM VisualSonics, Inc., Toronto, ON, Canada). A 2-dimensional (2D) parasternal short- and long-axis brightness (B-mode) of the mid-left ventricle (LV) was obtained at the level of the papillary muscles. Additionally, a 2D targeted motion-mode (M-mode) tracing was recorded to measure end diastolic and end systolic wall thicknesses and internal chamber dimensions. LV ejection fraction (%EF) and fractional shortening (%FS) were calculated as an index of LV systolic performance. Doppler-based flow velocity measurements were also taken to determine mitral valve E-wave/A-wave (MV E/A) ratios for diastolic LV function. MV E/A ratio marks changes in the peak velocity of blood flow from the LV during early diastole (E-wave) to the peak velocity of blood flow into the LV by atrial contraction during late diastole (A-wave). The MV E/A ratio represents LV filling velocity between systolic periods. Mice were maintained at ~1% isoflurane anesthesia during the echocardiography procedure. A minimum of 5 cardiac cycles were used to generate the data obtained. Heart measurements were conducted as described previously [58,59] after either 2- or 21-days of wash-out from Dox.

2.5. Tissue Collection

Following echocardiography measurements, mice were sacrificed via cervical dislocation followed by rapid decapitation and removal of heart. Hearts were collected, weighed, and tissues were flash-frozen on dry ice and stored at -80 °C until later biochemical analysis. Mid-ventricle sections were also fixed in 4% paraformaldehyde for histology.

2.5.1. Cardiac Histology

Paraformaldehyde-fixed ventricular tissues were paraffin-embedded and sectioned (5 μm). Sections were stained with polychromatic methylene blue (mast cells, 600 \times magnification) or picric acid Sirius red F3BA (PASR, collagen, 200 \times magnification). Mast cell counts were performed for each of the hearts ($n = 6–8$ /group), and mast cell counts were normalized to scanned images of the stained heart sections. A micrometer was included in each scan to calibrate units of area measurement [60]. Estimates of thick and thin collagen fibrils as a measure of fibrosis in the heart were conducted as previously described [46]. Due to the birefringent nature of the PASR stain, images of collagen fibrils from stained hearts were obtained by passing polarized light collagen, which refracted a distinct color based upon the size of the collagen fibrils: red and yellow (thick filaments) and green (thin filaments). Quantitative analysis was conducted using a light microscopy system

(Nikon Eclipse Ti2) with a video-based image-analyzer system. Triphasic analysis color thresholds were set to capture and generate a percent collagen content [(Red (0–40) Green (0–80) Blue (0–255)] per $20\times$ field within the specified RGB wavelength ranges separated from the background [Red (20–255) Green (40–255) Blue (35–255)]. Results are presented as the mean \pm SEM values computed from the average of $n = 25$ –35 individual measurements obtained from each heart. Cardiac vasculature, epicardium, and endocardium were avoided due to high levels of collagen content that do not accurately reflect myocardial interstitial collagen.

2.5.2. Western Blot

Proteins were isolated from hearts obtained from Tat(–) and Tat(+) mice. Tissues were minced in a Modified Hunter’s Buffer [MHB; 1% Triton X-100, 75 mM NaCl, 5 mM tris pH 7.4, 0.5 mM orthovanadate, 0.5 mM ECTA, 0.5 mM EGTA, 0.25% NP-40, and freshly added Halt Protease Inhibitor Cocktail (100 \times ; Thermo Fisher)]. Minced tissues were incubated on ice with MHB for 10 min, and tissue pieces were then sonicated. Samples were centrifuged for 15 min at $32,000\times g$ at 4 °C, and the supernatant was removed and stored at –80 °C. Protein concentrations were assessed using a bicinchoninic acid assay (BCA; Pierce Biotechnology) according to the manufacturer’s instructions. 25 μ g of protein per sample was loaded for Western blot analyses. Antibodies used were as follows: monoclonal α -smooth muscle actin (α -SMA; 43 kDa; 1:400; Sigma Aldrich 2547), RAGE (46 kDa; 1:400; Santa Cruz sc-365154), superoxide dismutase-1 (SOD-1; 23 kDa; 1:400; Santa Cruz Biotechnology sc-101523), and superoxide dismutase-2 (SOD-2; 25 kDa; 1:400; Santa Cruz Biotechnology sc-133134). β -tubulin (50 kDa; 1:400; Santa Cruz sc-398937) was used as a loading control. Western blots were visualized using an iBRIGHT imaging system (Thermo Fisher Scientific, Waltham, MA, USA).

Western Immunoblotting for GFAP: 25 μ g of heart lysate from Tat(–) and Tat(+) mice was reduced, heated, and run on a 4–20% Tris-glycine SDS-PAGE gel (Bio-Rad Laboratories, Hercules, CA, USA). The gel was run for 1 h at 25–30 mA/gel and then transferred to nitrocellulose membrane at 100 volts for 1 h at 4 °C. The membrane was blocked with Odyssey[®] Blocking Buffer in TBS (Licore, Inc, Lincoln, NJ, USA) for 1 h at room temperature. The membrane was then incubated with primary antibodies to GFAP at 1:1500 dilution (Millipore) or GAPDH at 1:1000 dilution (Santa Cruz) in a blocking buffer with gentle agitation at 4 °C overnight. The membrane was washed with TBST four times for 15 min each time. After washing, the membrane was incubated with an IRDye[®] 800CW goat anti-mouse against GFAP or IRDye[®] 680RD donkey anti-goat against GAPDH, both at 1:4000 dilution in blocking buffer for 1 h at room temperature. After three washes with TBST, the electroblotted proteins were detected via a LICOR-Odyssey CLX imager to visualize the protein bands.

2.5.3. RNA Isolation and Quantitative Real-Time Polymerase Chain Reaction

The ventricle and atrium regions of the mouse heart were isolated from each subject and homogenized in TRizol reagent according to manufacture protocol (Thermo Fisher Scientific) followed by Qiagen Clean up kit (Qiagen, Germantown, MD, USA). Total RNA concentration was determined by Nanodrop spectrophotometer (NanoDrop 2000c, Thermo Fisher Scientific). 1 μ g of RNA was used and cDNA was made using Revert Aid First Strand cDNA Synthesis (#K1651, Fisher Scientific). All primers were purchased from IDT (Coralville, IA, USA). qRT-PCR reactions were performed to measure Tat mRNA expression using a Bio-Rad CFX Connect Real-Time System (Bio-Rad, Hercules, CA, USA) in 96 well plates (Applied BioSystems, Fisher Scientific). 1 μ g of cDNA in a final volume of 25 μ L containing 400 nM primers using SYBR Green master mix (Thermo Fisher Scientific) was used for each reaction. The sequence for Tat primers was as follows: forward primer 5'-GCCCTGGAAGCATCCAGGAAGTC-3', reverse 5'-CGTCGCTGTCTCCGCTTCTTCCT-3'. The sequence for GAPDH primers was as follows: forward 5'-GGAAGCTCACTGGCATGGC-3', reverse 5'-TAGACGGCAGGTCAGGTCCA-3'.

The PCR thermal cycling reaction for each set of primers started with an initial denaturation at 95 °C for 10 min, step cycles at 95 °C for 5 s (denaturation), 58 °C for 10 s (annealing), 72 °C for 20 s (extension) for a total of 40 cycles followed by 72 °C for 5 min. qRT-PCR for the housekeeping gene, GAPDH, was performed in parallel for all reactions. Results are presented as the average of three independently conducted trials.

2.6. Statistical Analyses

Data for *tat* mRNA expression and echocardiography were analyzed via two-way analyses of variance (ANOVA). Mast cell counts, collagen content, and Western blot analyses were analyzed via one-way ANOVA. Fluo-4 AM data were analyzed via repeated measures ANOVA using treatment group as the between-subjects factor and time as the within-subjects factor. Group differences following main effects were assessed via Tukey's honestly significant difference *post hoc* tests. Interactions were delineated via simple main effects and main effect contrasts with α corrected for family wise error. Data were considered significant when $p \leq 0.05$. All analyses were performed using SAS StatView and the GraphPad Prism software.

3. Results

3.1. Tat Dysregulated Intracellular Calcium ($[Ca^{2+}]_i$) in Cultured Human Ventricular Cells

We first examined whether Tat exposure would alter Ca^{2+} homeostasis in a cultured AC16 cardiomyocyte cell line. Cultured human ventricular cells exposed to Tat (50 ng/mL; $n = 6$) demonstrated a significant increase Ca^{2+} influx in a time-dependent manner compared to vehicle treatment ($n = 3$; $F_{(135,945)} = 5.95$, $p < 0.05$; see * Figure 1). In Tat-treated cultures, all time-points following the addition of Tat at 30 s demonstrated a significant increase in $[Ca^{2+}]_i$ compared to control-treated cultures.

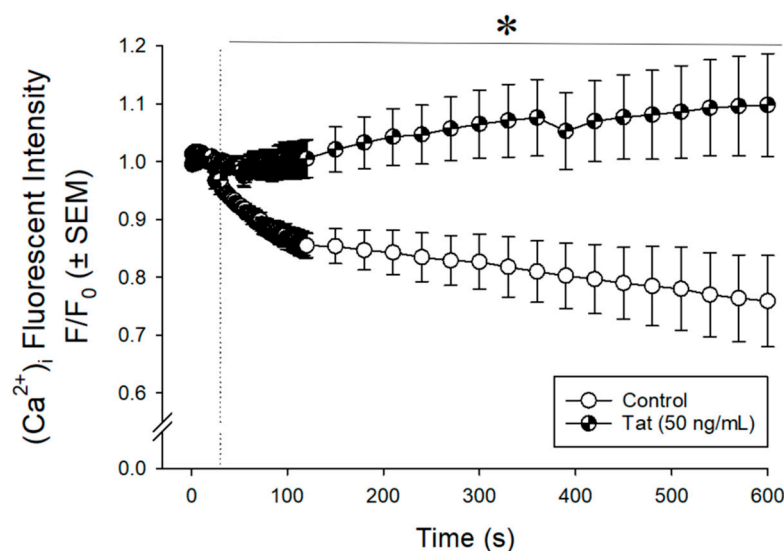


Figure 1. Intracellular Calcium Levels in Cultured Cardiomyocytes. Cells were incubated with Fluo-4 AM and intracellular calcium was measured over 10 min (every second for the first 2 min; and every 30 s for the next 8 min). Tat (50 ng/mL) or vehicle was applied at 30 s. * Indicates Tat-treated cells significantly differed from control at all times post 30 s; $p \leq 0.05$, repeated measures two-way ANOVA.

3.2. Tat Induction Increased Tat mRNA Levels in the Whole Heart among Adult Male Mice

We assessed the effect of conditional HIV-1 Tat induction on the presence of *tat* transgene within the heart of adult male mice via qRT-PCR. Transgenic HIV-1 Tat mice, ($n_{Tat(-)} = 2$, $n_{Tat(+)} = 3$) were injected with Dox (56 mg/kg) for 5 days with 2 days of washout. There was a main effect of Tat genotype, wherein Tat(+) mice had greater *tat* mRNA expression in either the atrial or ventricular heart chambers compared to control Tat(-) mice

($F_{(1,6)} = 18.27, p \leq 0.05$; see * Figure 2). We did not observe differences in Tat expression between heart chambers, atrial and ventricular. Given that Tat protein expression is driven by GFAP in this mouse model, we did confirm the expression of GFAP protein expression within the heart of Tat(−) and Tat(+) mice (Figure S1). Thus, *tat* mRNA expression was detected in the whole heart of adult mice.

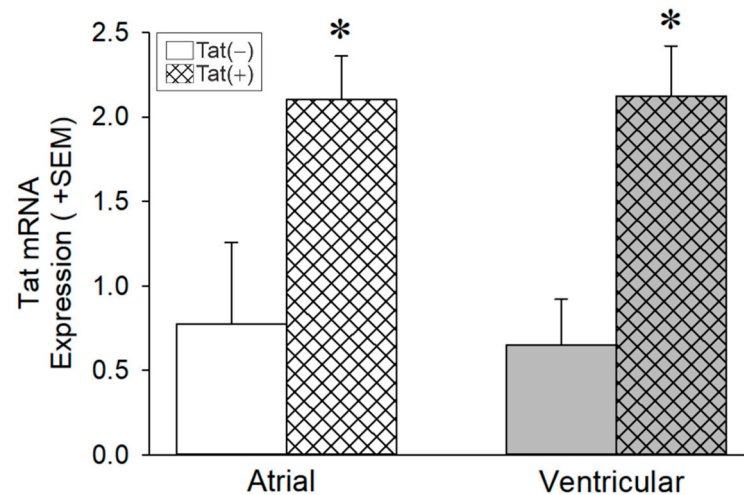


Figure 2. *tat* mRNA Expression in the Heart. *tat* mRNA expression was detected in the whole heart of Tat(+) mice (hatched bars) compared to their control Tat(−) mice (open bars; $n = 2-3$ per group). * indicates a main effect of genotype wherein Tat(+) mice differ from Tat(−) controls; $p < 0.05$; two-way ANOVA.

3.3. Tat Induction Did Not Alter Cardiac Function among Adult Mice

Given the acute changes observed for Tat to increase $[Ca^{2+}]_i$, we next investigated whether Tat expression in the heart would interfere with myocardium function using Tat-transgenic male and female adult mice. Neither Tat genotype nor exposure to Dox significantly influenced cardiac physiological function when assessed by B-mode or M-mode using ultrasound (Table 1). The heart rates and the proportion of ejection fraction remained unchanged across all groups (Table 1). We did not observe any alteration of cardiac function between saline (Table 1, Figure 3a,b) or Dox-treated (56 mg/kg) mice (Table 1, Figure 3c,d).

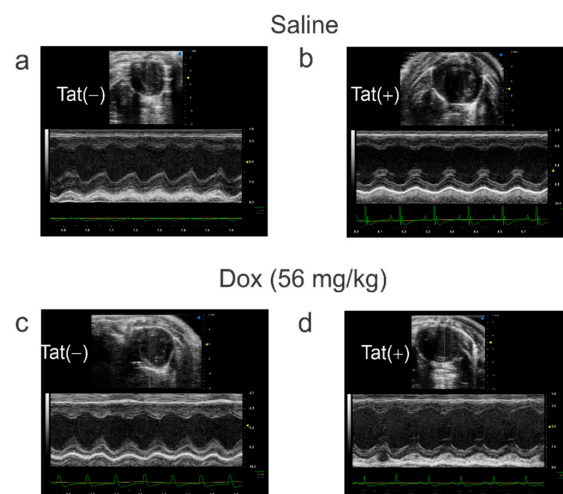


Figure 3. Two-Dimensional Echocardiographic Images Measured by Ultrasound. Tat expression did not alter cardiac function among adult Tat-transgenic mice [Tat(+)] compared to their non-Tat-expressing age-matched counterparts [Tat(−)]. (a) Tat(−) mice treated with saline, (b) Tat(+) mice treated with saline, (c) Tat(−) mice treated with Dox, (d) Tat(+) mice treated with Dox.

Table 1. Morphological and cardiac functional assessments by echocardiogram parameters including brightness- (B-mode) and motion-mode (M-mode) measurements among HIV-1 Tat transgenic mice treated with saline or Dox.

Gender	Male				Female			
Tat Genotype	Tat(−)	Tat(+)	Tat(−)	Tat(+)	Tat(−)	Tat(+)	Tat(−)	Tat(+)
n-value	8	13	5	15	11	12	24	22
Treatment	Saline		Dox 56 mg/kg		Saline		Dox 56 mg/kg	
HR (bpm)	454.09 ± 49.21	488.37 ± 52.74	473.52 ± 45.52	477.33 ± 70.09	465.07 ± 88.05	465.07 ± 88.05	470.70 ± 53.07	483.51 ± 98.17
	B-mode				B-mode			
SV (μL)	18.21 ± 3.44	24.38 ± 4.82	20.04 ± 7.98	19.83 ± 5.45	17.69 ± 4.13	17.29 ± 3.24	19.75 ± 6.26	20.20 ± 5.63
%EF	48.66 ± 5.61	50.33 ± 9.22	49.71 ± 8.49	47.49 ± 9.67	44.52 ± 9.78	53.31 ± 11.05	52.02 ± 9.22	55.28 ± 7.76
%FS	15.10 ± 4.44	14.01 ± 5.81	13.11 ± 5.92	12.18 ± 4.20	10.11 ± 3.98	12.69 ± 4.22	13.45 ± 5.18	13.52 ± 5.76
CO (mL/min)	8.02 ± 1.59	11.73 ± 1.73	9.14 ± 2.77	9.40 ± 3.07	8.23 ± 2.70	8.31 ± 2.67	9.16 ± 2.77	9.89 ± 3.68
Area (mm ²)	11.91 ± 3.67	14.47 ± 3.70	13.84 ± 5.62	12.75 ± 3.51	14.45 ± 4.01	9.98 ± 2.13	10.99 ± 2.00	11.73 ± 2.73
Area, s (mm ²)	11.10 ± 2.32	13.39 ± 3.24	12.18 ± 4.27	12.33 ± 2.69	12.66 ± 2.35	9.66 ± 1.75	10.68 ± 1.82	10.15 ± 2.05
Area, d (mm ²)	16.73 ± 2.54	20.25 ± 2.86	17.61 ± 5.13	18.16 ± 3.07	17.91 ± 2.48	15.20 ± 1.31	16.81 ± 2.62	16.39 ± 2.51
Volume (μL)	24.10 ± 12.14	30.55 ± 11.56	29.94 ± 17.20	24.25 ± 10.25	30.18 ± 13.00	17.29 ± 6.68	18.38 ± 5.05	22.25 ± 9.68
Volume, s (μL)	20.41 ± 7.06	26.70 ± 10.18	23.74 ± 11.05	22.58 ± 7.45	23.48 ± 6.73	16.03 ± 5.51	17.48 ± 4.38	16.60 ± 5.12
Volume, d (μL)	38.62 ± 9.94	51.07 ± 11.39	20.04 ± 7.98	42.41 ± 10.55	41.17 ± 8.66	33.31 ± 5.44	37.24 ± 8.27	36.79 ± 9.44
	M-mode				M-mode			
%EF	63.15 ± 14.73	55.27 ± 16.51	55.42 ± 6.98	62.91 ± 10.61	61.30 ± 6.39	61.77 ± 11.27	63.48 ± 7.18	64.55 ± 6.62
%FS	34.77 ± 10.05	29.97 ± 11.94	28.46 ± 4.31	33.85 ± 7.51	32.28 ± 4.49	33.21 ± 7.07	33.70 ± 5.26	34.45 ± 4.78
IVS, d (mm)	1.08 ± 0.19	0.99 ± 0.23	0.75 ± 0.05	1.16 ± 0.26	0.89 ± 0.21	1.04 ± 0.24	1.13 ± 0.24	0.91 ± 0.20
IVS, s (mm)	1.48 ± 0.21	1.38 ± 0.38	1.07 ± 0.06	1.50 ± 0.28	1.30 ± 0.23	1.37 ± 0.21	1.56 ± 0.25	1.35 ± 0.25
LVID, d (mm)	3.27 ± 0.36	3.65 ± 0.59	3.65 ± 0.32	3.28 ± 0.39	3.36 ± 0.36	3.07 ± 0.30	3.09 ± 0.37	3.12 ± 0.37
LVID, s (mm)	2.15 ± 0.49	2.64 ± 0.78	2.62 ± 0.31	2.19 ± 0.38	2.28 ± 0.31	2.04 ± 0.27	2.06 ± 0.32	2.04 ± 0.32
LVPW, d (mm)	1.22 ± 0.27	1.01 ± 0.23	0.91 ± 0.16	1.08 ± 0.20	0.97 ± 0.31	1.02 ± 0.20	1.16 ± 0.31	1.09 ± 0.28
LVPW, s (mm)	1.57 ± 0.33	1.33 ± 0.25	1.29 ± 0.20	1.43 ± 0.23	1.30 ± 0.27	1.37 ± 0.20	1.46 ± 0.28	1.43 ± 0.25

HR: heart rate; SV: stroke volume; EF: ejection fraction; FS: fractional shortening; CO: cardiac output; s: systolic; D: diastolic; IVS: interventricular septum; LVID: left ventricle inner dimension; LVPW: left ventricular posterior wall; Dox: doxycycline.

3.4. Tat Induction Upregulated RAGE and SOD-2 in Ventricular Tissue of Adult Mice

To further investigate the effect of Tat exposure on the cardiac function, we examined the levels of RAGE, α -SMA, and antioxidant proteins (SOD-1 and SOD-2) within the hearts of male Tat-transgenic mice. Inducing Tat with Dox significantly increased RAGE expression in the heart [$F_{(3,17)} = 7.426$, $p \leq 0.05$; see *, Figure 4a]. Neither Tat nor treatment with Dox influenced expression of α -SMA (Figure 4b) or the cytosolic antioxidant copper/zinc-SOD-1 (Figure 4c). However, Tat expression induced by Dox significantly upregulated the mitochondrial antioxidant magnesium-SOD-2 [$F_{(3,18)} = 4.359$, $p \leq 0.05$; see * Figure 4d). Dox alone did not account for changes in the expression of any analyte assessed, given that Dox-treated Tat(−) mice did not differ from saline-treated Tat(−) mice on any measure (Figure 4a–d). Thus, Tat induction significantly influenced the expression of RAGE and mitochondrial antioxidant SOD-2 in adult mice despite exerting no functional changes within the hearts.

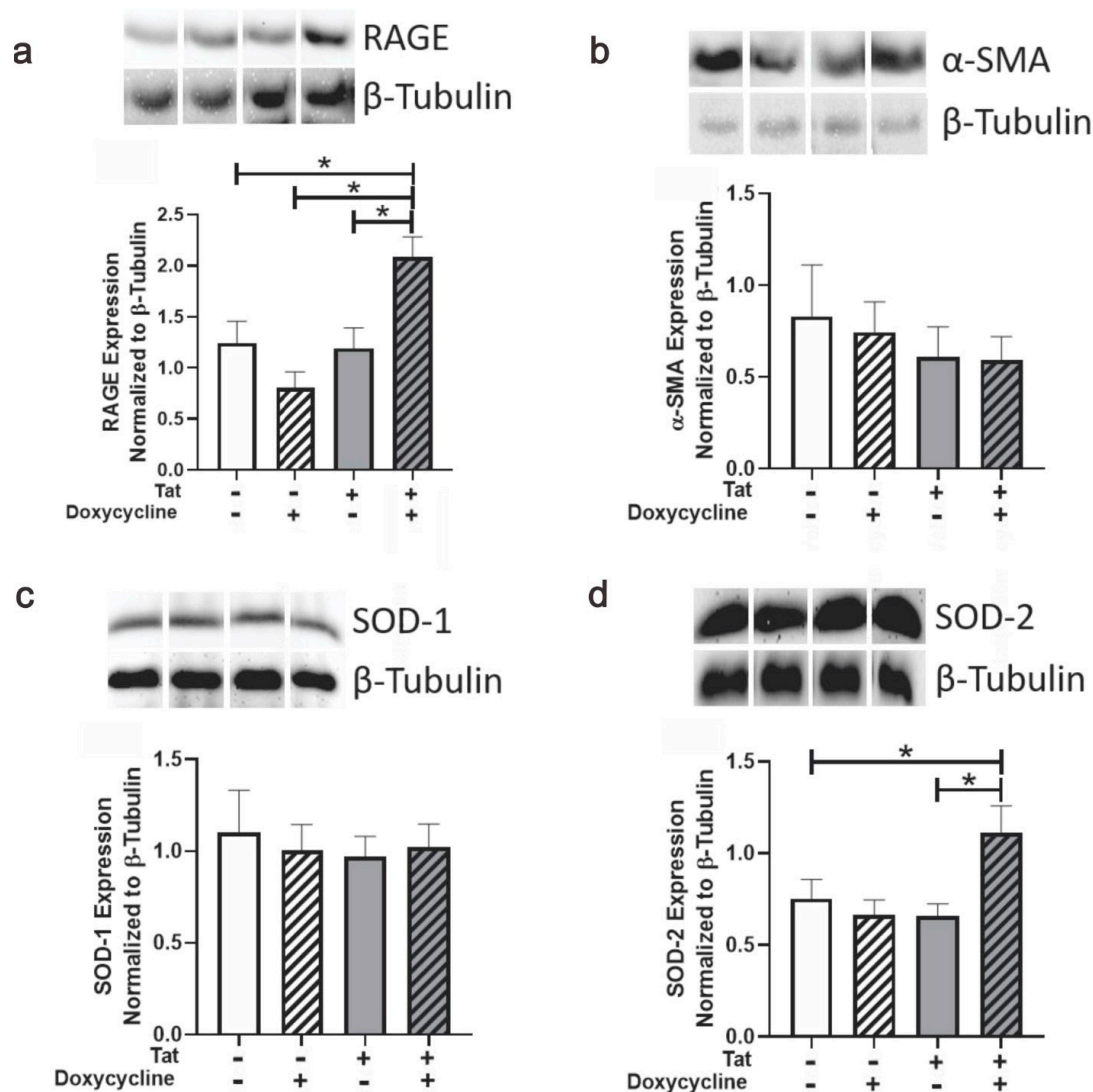


Figure 4. Effect of Tat Expression on the Cardiac Biomarkers of Transgenic Tat Adult Male Mice. Compared to Tat(−) controls, Tat(+) mice (n = 7–8/group) demonstrated upregulation of (a) RAGE and (d) SOD-2, but not (b) α -SMA or (c) SOD-1; * $p \leq 0.05$; one-way ANOVA followed by Tukey’s HSD.

3.5. Tat Exposure Altered Mast Cell Numbers and Collagen Deposition within Ventricular Tissue of Mice

We also assessed the effect of Tat induction on the cardiac extracellular matrix. Unexpectedly, the mast cell population was upregulated in Tat(+) mice, irrespective of DOX exposure [$F_{(3,22)} = 8.971$, $p < 0.05$; see *, Figure 5a,b). Similarly, collagen deposition was increased in the ventricular tissue of Tat(+) mice administered saline, but not those administered Dox, which may have exerted an ameliorating effect [$F_{(3,24)} = 9.958$, $p < 0.05$; see * Figure 5c,d)].

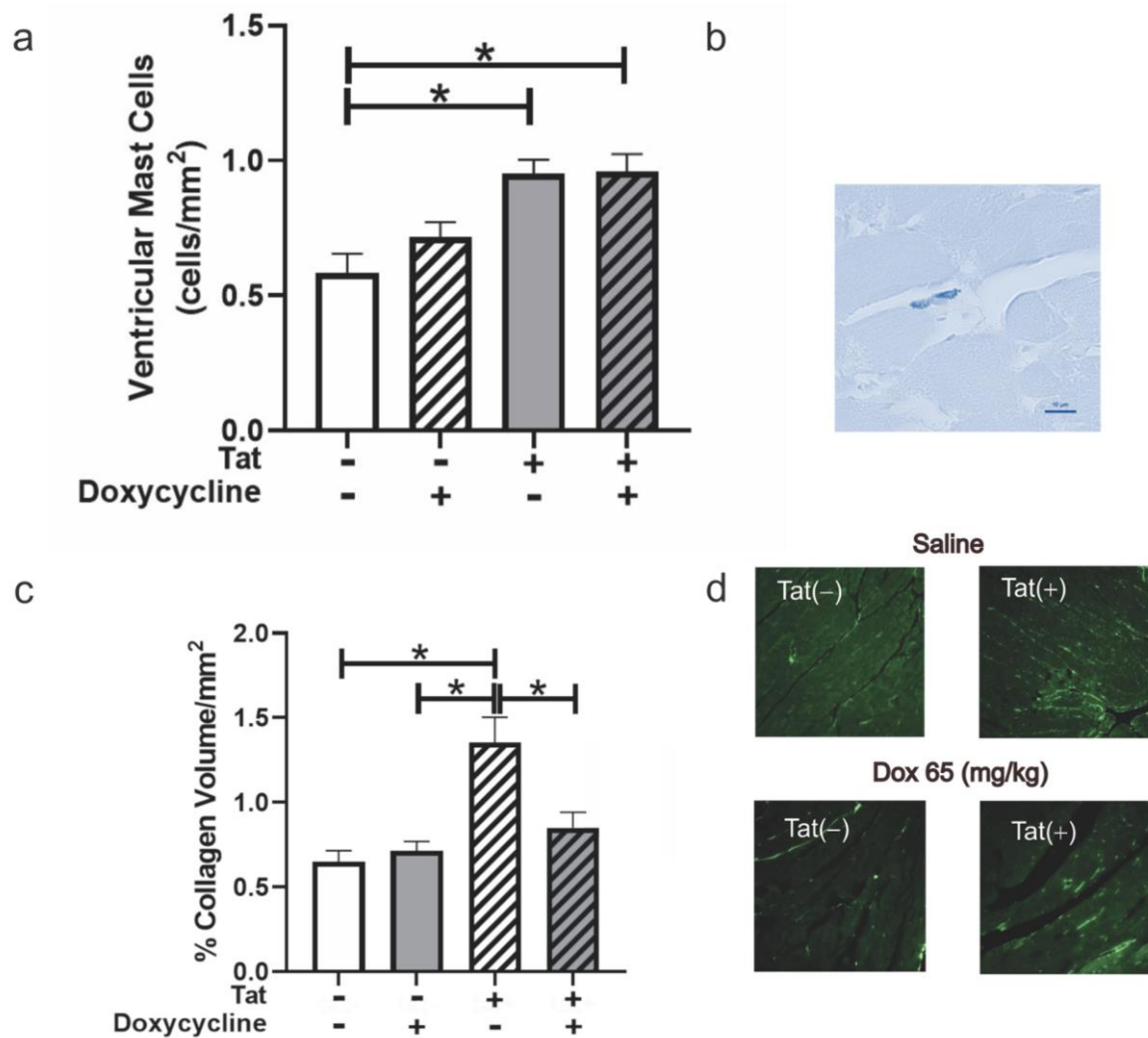


Figure 5. Mast Cells and Collagen Deposition in the Heart of Tat-Transgenic Adult Male Mice or their non-Tat-expressing counterparts. Tat expression influenced pro-inflammatory mast cell releases and extracellular collagen deposition in Tat(+) mice (n = 7–8/group). (a) Mast cell numbers and (b) a representative photomicrograph of stained mast cells. (c) Proportional collagen deposition and (d) PASR-stained representative images; * $p \leq 0.05$; one-way ANOVA followed by Tukey's HSD. Scale bar = 10 μm .

4. Discussion

In the era of antiretroviral therapy, CVDs occur prematurely and independently of traditional risk factors among PLWH [61–63]. The underlying mechanisms by which HIV contributes to CVDs are multifactorial [64–68]. However, it is unknown how viral proteins, including Tat, contribute to CVDs. This study is the first, to our knowledge, to investigate the effect of GFAP-driven Tat expression on the pathogenesis of cardiac dysfunction. In cultured human cardiomyocytes, Tat increased $[\text{Ca}^{2+}]_i$ demonstrating its capacity to exert acute effects on ion flux in heart cells. These findings have been demonstrated to be responsible for changes in cardiac contractility and dysfunction [69,70]. Although the *tat* transgene was detected in the atrium and ventricular chambers of the heart in Tat(+) mice, we did not observe an overall significant change in cardiac function. However, earlier biochemical changes in the heart indicative of cardiac dysfunction were detected. Tat(+) mice demonstrated an increased expression of RAGE and the mitochondrial antioxidant, SOD-2. Prior studies have established an association between SOD-2 upregulation and mitochondrial dysfunction [71,72], resulting in cardiac abnormalities [73–75]. Together, these findings support the notion that Tat exposure in adult mice promotes changes in cardiac

protein markers consistent with mitochondrial dysfunction. These events may occur prior to cardiac structural and/or functional changes. Thus, these findings suggest that Tat is sufficient to induce changes in the myocardium of adult HIV-1 Tat-expressing mice.

Echocardiographic abnormalities characterized by functional and structural changes are commonly reported among young adults living with HIV [11,74]. Therefore, PLWH are more vulnerable to develop cardiac dysfunction [75–79] and LV hypertrophy [75,78,79]. Independent of HIV, several underlying factors are associated with diastolic dysfunction, and metabolic disorders [75,80–83]. In this work, we demonstrated that Tat exposure did not significantly alter diastolic or systolic function in Tat-transgenic mice at a young adult age. Our data are consistent with prior preclinical findings using Tat-exposed young mice that reported no functional change in heart physiology [84,85]. However, LV dysfunction was observed at 6 months of age among transgenic mice that expressed Tat in the myocardium, concurrent with diastolic and systolic dysfunction [84,85]. These findings support the notion that cardiac biomarkers associated with Tat-mediated abnormalities may appear at younger ages and precede ventricular dysfunction and heart remodeling/failure. Further studies are required to assess these changes in an older cohort of mice. As well, greater investigation of the potential Tat-mediated mechanisms responsible for CVDs, including the alteration of mitochondrial function and Ca^{2+} homeostasis, should be explored.

Mitochondrial function plays a vital role in maintaining cardiac function and the buffering of Ca^{2+} [86–88]. Alterations in mitochondrial structure and/or function contribute to numerous cardiomyopathies [34,71,86]. Studies have demonstrated that Tat-induced mitochondrial dysfunction occurs in cultured neurons [89,90]. Similarly, Tat effects on mitochondrial function can also occur in the myocardium. In the Tat-targeted myocardial model, the overexpression of Tat was associated with mitochondrial damage, including swelling, cristae and matrix disruption, and incomplete fusion [84,86]. Tat also impaired mitochondrial quality control, reduced bioenergetic capacity, disrupted mitochondrial membrane potential, and amplified ROS formation in cultured cardiomyocytes [34]. We and others have found that Tat upregulates $[\text{Ca}^{2+}]_i$ in cultured cardiomyocytes, which is expected to increase the risk of CVDs [34,91,92]. Although the underlying mechanisms of Tat-induced mitochondrial injury are not fully understood, changes in redox status might contribute to Tat-induced mitochondrial dysfunction in cultured cardiomyocytes and astrocytes. However, pretreatment with superoxide dismutase attenuated Tat's effect on astrocytes [93]. Manganese SOD-2 is an antioxidant-protecting protein localized solely in the mitochondria (mitochondrial matrix and intermembrane space; [94–96]). SOD-2 deficiency contributes to cardiac mitochondrial injury, dilated heart chambers [97], a higher incidence of ventricular remodeling, and cardiac fibrosis [73,74]. A higher SOD-2 level was reported in Alzheimer's disease, which would be considered a compensatory response to attenuate oxidative stress damage [98,99]. Interactions with additional virotoxic HIV proteins may also contribute to CVDs. In support, the level and activity of SOD-2 were augmented in cultured astrocytes in response to the HIV envelope protein, gp120 [100]. In this study, we find increased SOD-2 expression, which may be a compensatory mechanism in response to Tat-induced mitochondrial dysfunction and the failure of Ca^{2+} handling in cardiomyocytes. In addition to Tat-mediated mitochondrial injury, we demonstrated increased mast cell numbers in the cardiac tissue. Mast cell-derived proinflammatory substances such as histamines, cytokines, leukotrienes, and prostaglandins promote cardiac fibrosis during long-term heart remodeling [100–102]. Thus, these findings suggest the association between immune dysregulation and CVD in HIV. In support of this, innate immune activation, including activated monocytes and cardiac macrophages, contributes to CVDs [103,104]. Accordingly, elevated SOD-2 levels might attenuate Tat-mediated mast cell activation at younger ages. However, the impact of prolonged mast cell activation is not well understood. Together, the capacity of Tat to induce cardiomyopathies via mitochondrial injury, overload of Ca^{2+} , and increased mast cell number may be an important contributor to cardiac dysfunction in HIV.

RAGE also plays an important role in the pathology of several age-related comorbidities, such as CVDs [104], Alzheimer's disease [105], and osteoarthritis [106]. RAGE has been demonstrated to be upregulated with aging and accumulates mainly within the heart [107]. Accordingly, RAGE is also involved in mitochondrial dysfunction, including impaired mitochondrial biogenesis, enhanced oxidative stress, altered mitochondrial membrane potential, increased mtDNA damage, and induced mitochondrial death [108–111]. In addition to mitochondrial damage, RAGE contributes to aortic structural changes characterized by increased collagen deposition in rodents [108,112]. Recent studies have indicated that HIV-1 Tat-induced RAGE expression within the blood–brain barrier accelerates amyloid beta deposition [36–38]. The influence of RAGE within the heart could also be an underlying mechanism for Tat-induced CVDs. Consistent with prior findings, we observed Tat exposure to significantly increased RAGE expression in the hearts of young adult male mice, which might be an early biomarker for increased CVD risk. Inhibiting RAGE signaling might serve as a potential therapeutic intervention in PLWH to lower the risk of premature cardiovascular disorders.

The present data must be considered in relation to some caveats. Mast cell number and collagen deposition increased in Tat(+) mice irrespective of Dox treatment. Given that Dox exerts anti-inflammatory effects on its own, its administration may have masked some effects. In support, mast cells were elevated in Tat(+) mice administered saline which could be due to 'leaky' expression of Tat in this model [113], but this was not further elevated by Dox administration. Likewise, collagen deposition increased in uninduced Tat(+) mice, Dox administration completely abrogated this effect. The temporal nature of Tat induction by Dox may also play a role in these surprising effects. As such, these findings should also be replicated in Dox-independent animal models.

5. Conclusions

These data demonstrate that GFAP-driven Tat expression promotes cardiac abnormalities among adult mice. In support, we determined *tat* mRNA expression in the whole heart concurrent with the dysregulation of calcium homeostasis, the upregulation of RAGE, mitochondrial antioxidant SOD-2, and the mast cell-derived inflammatory response. However, we observed no changes in cardiac functions at young ages. Therefore, these alterations within the myocardium may serve as early biomarkers of CVD before developing cardiac dysfunction among PLWH.

Supplementary Materials: The following supporting information can be downloaded at: <https://www.mdpi.com/xxx/s1>, Figure S1: Expression of GFAP in the heart of Tat-transgenic mice.

Author Contributions: A.N.Q.: Writing—original draft, Data curation, Writing—original draft, Writing—review and editing. N.S.W.: Data curation, E.R.H.: Data curation. F.M.: Data curation. J.A.S.J.: Conceptualization, Funding Acquisition, Data curation, Formal analysis, Writing—original draft, Writing—review and editing. J.J.P.: Conceptualization, Funding acquisition, Data curation, Formal analysis, Writing—original draft, Writing—review and editing. All authors have read and agreed to the published version of the manuscript.

Funding: This work was supported by funds from the University of Mississippi and the National Institutes of Health: R01 DA052851 (JJP). We thank Zia Shariat-Madar for the use of equipment in determining RNA expression.

Institutional Review Board Statement: The study was conducted according to the ethical guidelines defined by National Institute of Health (NIH Publication No. 85-23) and approved by the Institutional Animal Care and Use Committee (IACUC) at The University of Mississippi (Protocol #18-004 and 21-005; approved October 2017 and October 2020, respectively).

Informed Consent Statement: Not applicable.

Data Availability Statement: Data available upon request.

Conflicts of Interest: The authors declare no conflict of interest. The funders had no role in the design of the study, data collection, data analyses, data interpretation, the writing of the manuscript, or in the decision to publish the results.

References

1. Saylor, D.; Dickens, A.; Sacktor, N.; Haughey, N.; Slusher, B.; Pletnikov, M.; Mankowski, J.L.; Brown, A.; Volsky, D.J.; McArthur, J.C. HIV-associated neurocognitive disorder—Pathogenesis and prospects for treatment. *Nat. Rev. Neurol.* **2016**, *12*, 234–248. [[CrossRef](#)]
2. Thakur, K.T.; Boubour, A.; Saylor, D.; Das, M.; Bearden, D.R.; Birbeck, G.L. Global HIV neurology. *AIDS* **2019**, *33*, 163–184. [[CrossRef](#)] [[PubMed](#)]
3. Veenhuis, R.T.; Clements, J.E.; Gama, L. HIV Eradication Strategies: Implications for the Central Nervous System. *Curr. HIV/AIDS Rep.* **2019**, *16*, 96–104. [[CrossRef](#)] [[PubMed](#)]
4. Guaraldi, G.; Orlando, G.; Zona, S.; Menozzi, M.; Carli, F.; Garlassi, E.; Berti, A.; Rossi, E.; Roverato, A.; Palella, F. Premature Age-Related Comorbidities Among HIV-Infected Persons Compared with the General Population. *Clin. Infect. Dis.* **2011**, *53*, 1120–1126. [[CrossRef](#)]
5. Onen, N.F.; Overton, E.T. A review of premature frailty in HIV-infected persons; another manifestation of HIV-related accelerated aging. *Curr. Aging Sci.* **2011**, *1*, 33–41. [[CrossRef](#)]
6. Pathai, S.; Bajillan, H.; Landay, A.L.; High, K.P. Is HIV a Model of Accelerated or Accentuated Aging? *J. Gerontol. Ser. A* **2014**, *69*, 833–842. [[CrossRef](#)]
7. Sackoff, J.E.; Hanna, D.B.; Pfeiffer, M.R.; Torian, L.V. Causes of death among persons with AIDS in the era of highly active antiretroviral therapy: New York City. *Ann. Intern. Med.* **2006**, *6*, 397–406. [[CrossRef](#)]
8. Triant, V.A.; Brown, T.T.; Lee, H.; Grinspoon, S.K. Fracture Prevalence among Human Immunodeficiency Virus (HIV)-Infected Versus Non-HIV-Infected Patients in a Large U.S. Healthcare System. *J. Clin. Endocrinol. Metab.* **2008**, *93*, 3499–3504. [[CrossRef](#)]
9. Tripathy, S.K.; Agrawala, R.K.; Baliarsingha, A. Endocrine alterations in HIV-infected patients. *Indian J. Endocrinol. Metab.* **2015**, *19*, 143–147. [[CrossRef](#)]
10. Neuhaus, J.; Jacobs, D.R., Jr.; Baker, J.V.; Calmy, A.; Duprez, D.; La Rosa, A.; Kuller, L.H.; Pett, S.L.; Ristola, M.; Ross, M.J.; et al. Markers of Inflammation, Coagulation, and Renal Function Are Elevated in Adults with HIV Infection. *J. Infect. Dis.* **2010**, *201*, 1788–1795. [[CrossRef](#)]
11. Freiberg, M.S.; Chang, C.-C.H.; Skanderson, M.; Patterson, O.V.; DuVall, S.L.; Brandt, C.A.; So-Armah, K.A.; Vasan, R.S.; Oursler, K.A.; Gottdiener, J.; et al. Association Between HIV Infection and the Risk of Heart Failure with Reduced Ejection Fraction and Preserved Ejection Fraction in the Antiretroviral Therapy Era. *JAMA Cardiol.* **2017**, *2*, 536–546. [[CrossRef](#)] [[PubMed](#)]
12. Monsuez, J.-J.; Escaut, L.; Teicher, E.; Charniot, J.-C.; Vittecoq, D. Cytokines in HIV-associated cardiomyopathy. *Int. J. Cardiol.* **2007**, *120*, 150–157. [[CrossRef](#)] [[PubMed](#)]
13. Durand, M.; Sheehy, O.; Baril, J.-G.; Leloir, J.; Tremblay, C.L. Association Between HIV Infection, Antiretroviral Therapy, and Risk of Acute Myocardial Infarction: A Cohort and Nested Case–Control Study Using Québec’s Public Health Insurance Database. *JAIDS J. Acquir. Immune Defic. Syndr.* **2011**, *57*, 245–253. [[CrossRef](#)] [[PubMed](#)]
14. Lang, S.; Mary-Krause, M.; Cotte, L.; Gilquin, J.; Partisani, M.; Simon, A.; Boccara, F.; Costagliola, D. Impact of Individual Antiretroviral Drugs on the Risk of Myocardial Infarction in Human Immunodeficiency Virus–Infected Patients A Case-Control Study Nested Within the French Hospital Database on HIV ANRS Cohort CO4 Antiretroviral Drugs, Risk of MI, and HIV. *Arch. Intern. Med.* **2010**, *170*, 1228–1238. [[CrossRef](#)]
15. Kaplan, R.C.; Kingsley, L.A.; Sharrett, A.R.; Li, X.; Lazar, J.; Tien, P.C.; Mack, W.J.; Cohen, M.H.; Jacobson, L.; Gange, S.J. Ten-Year Predicted Coronary Heart Disease Risk in HIV-Infected Men and Women. *Clin. Infect. Dis.* **2007**, *45*, 1074–1081. [[CrossRef](#)]
16. Savès, M.; Chêne, G.; Ducimetière, P.; Lepout, C.; Le Moal, G.; Amouyel, P.; Arveiler, D.; Ruidavets, J.-B.; Reynes, J.; Bingham, A.; et al. Risk Factors for Coronary Heart Disease in Patients Treated for Human Immunodeficiency Virus Infection Compared with the General Population. *Clin. Infect. Dis.* **2003**, *37*, 292–298. [[CrossRef](#)]
17. Vittecoq, D.; Escaut, L.; Chironi, G.; Teicher, E.; Monsuez, J.J.; Andrejak, M.; Simon, A. Coronary heart disease in HIV-infected patients in the highly active antiretroviral treatment era. *AIDS* **2003**, *17*, S70–S76. [[CrossRef](#)]
18. Tseng, Z.H.; Secemsky, E.A.; Dowdy, D.; Vittinghoff, E.; Moyers, B.; Wong, J.K.; Havlir, D.V.; Hsue, P.Y. Sudden Cardiac Death in Patients with Human Immunodeficiency Virus Infection. *J. Am. Coll. Cardiol.* **2012**, *59*, 1891–1896. [[CrossRef](#)]
19. Narla, V.A. Sudden cardiac death in HIV-infected patients: A contemporary review. *Clin. Cardiol.* **2021**, *44*, 316–321. [[CrossRef](#)]
20. Mensah, G.A.; Roth, G.A.; Fuster, V. The Global Burden of Cardiovascular Diseases and Risk Factors: 2020 and beyond. *J. Am. Coll. Cardiol.* **2019**, *74*, 2529–2532. [[CrossRef](#)]
21. Feinstein, M.J.; Hsue, P.Y.; Benjamin, L.; Bloomfield, G.S.; Currier, J.S.; Freiberg, M.S.; Grinspoon, S.K.; Levin, J.; Longenecker, C.T.; Post, W.S. Characteristics, Prevention, and Management of Cardiovascular Disease in People Living With HIV: A Scientific Statement from the American Heart Association. *Circulation* **2019**, *140*, e98–e124. [[CrossRef](#)] [[PubMed](#)]
22. Smit, M.; Brinkman, K.; Geerlings, S.; Smit, C.; Thyagarajan, K.; van Sighem, A.; de Wolf, F.; Hallett, T.B. Future challenges for clinical care of an ageing population infected with HIV: A modelling study. *Lancet Infect. Dis.* **2015**, *15*, 810–818. [[CrossRef](#)]

23. Esser, S.; Gelbrich, G.; Brockmeyer, N.; Goehler, A.; Schadendorf, D.; Erbel, R.; Neumann, T.; Reinsch, N. Prevalence of cardiovascular diseases in HIV-infected outpatients: Results from a prospective, multicenter cohort study. *Clin. Res. Cardiol.* **2013**, *102*, 203–213. [[CrossRef](#)] [[PubMed](#)]
24. Johnson, T.P.; Patel, K.; Johnson, K.R.; Maric, D.; Calabresi, P.A.; Hasbun, R.; Nath, A. Induction of IL-17 and nonclassical T-cell activation by HIV-Tat protein. *Proc. Natl. Acad. Sci. USA* **2013**, *110*, 13588–13593. [[CrossRef](#)]
25. Henderson, L.J.; Johnson, T.P.; Smith, B.R.; Reoma, L.; Santamaria, U.A.; Bachani, M.; DeMarino, C.; Barclay, R.A.; Snow, J.; Sacktor, N.; et al. Presence of Tat and transactivation response element in spinal fluid despite antiretroviral therapy. *AIDS* **2019**, *33* (Suppl. S2), S145–S157. [[CrossRef](#)]
26. Das, A.T.; Harwig, A.; Berkhout, B. The HIV-1 Tat Protein Has a Versatile Role in Activating Viral Transcription. *J. Virol.* **2011**, *85*, 9506–9516. [[CrossRef](#)] [[PubMed](#)]
27. Re, M.C.; Furlini, G.; Vignoli, M.; Ramazzotti, E.; Roderigo, G.; De Rosa, V.; Zauli, G.; Lolli, S.; Capitani, S.; La Placa, M. Effect of Antibody to HIV-1 Tat Protein on Viral Replication in Vitro and Progression of HIV-1 Disease in Vivo. *J. Acquir. Immune Defic. Syndr. Hum. Retrovirol.* **1995**, *10*, 408–416. [[CrossRef](#)]
28. Liu, K.; Chi, D.S.; Li, C.; Hall, H.K.; Milhorn, D.M.; Krishnaswamy, G. HIV-1 Tat protein-induced VCAM-1 expression in human pulmonary artery endothelial cells and its signaling. *Am. J. Physiol. Cell. Mol. Physiol.* **2005**, *289*, L252–L260. [[CrossRef](#)]
29. Duan, M.; Yao, H.; Hu, G.; Chen, X.; Lund, A.K.; Buch, S. HIV Tat Induces Expression of ICAM-1 in HUVECs: Implications for miR-221/-222 in HIV-Associated Cardiomyopathy. *PLoS ONE* **2013**, *8*, e60170. [[CrossRef](#)]
30. Zhan, J.; Qin, S.; Lu, L.; Hu, X.; Zhou, J.; Sun, Y.; Yang, J.; Liu, Y.; Wang, Z.; Tan, N.; et al. miR-34a is a common link in both HIV- and antiretroviral therapy-induced vascular aging. *Aging* **2016**, *8*, 3298–3310. [[CrossRef](#)]
31. Ben Haij, N.; Planès, R.; Leghmari, K.; Serrero, M.; Delobel, P.; Izopet, J.; BenMohamed, L.; Bahraoui, E. HIV-1 Tat Protein Induces Production of Proinflammatory Cytokines by Human Dendritic Cells and Monocytes/Macrophages through Engagement of TLR4-MD2-CD14 Complex and Activation of NF- κ B Pathway. *PLoS ONE* **2015**, *10*, e0129425. [[CrossRef](#)] [[PubMed](#)]
32. Cota-Gomez, A.; Flores, N.C.; Cruz, C.; Casullo, A.; Aw, T.Y.; Ichikawa, H.; Schaack, J.; Scheinman, R.; Flores, S.C. The Human Immunodeficiency Virus-1 Tat Protein Activates Human Umbilical Vein Endothelial Cell E-selectin Expression via an NF- κ B-dependent Mechanism. *J. Biol. Chem.* **2002**, *277*, 14390–14399. [[CrossRef](#)] [[PubMed](#)]
33. Meng, Z.; Hernandez, R.; Liu, J.; Gwag, T.; Lu, W.; Hsiai, T.K.; Kaul, M.; Zhou, T.; Zhou, C. HIV Protein Tat Induces Macrophage Dysfunction and Atherosclerosis Development in Low-Density Lipoprotein Receptor-Deficient Mice. *Cardiovasc. Drugs Ther.* **2022**, *36*, 201–215. [[CrossRef](#)] [[PubMed](#)]
34. Tahir, F.G.; Shanmughapriya, S.; Ahooyi, T.M.; Knezevic, T.; Gupta, M.K.; Kontos, C.D.; McClung, J.M.; Madesh, M.; Gordon, J.; Feldman, A.M.; et al. Dysregulation of mitochondrial bioenergetics and quality control by HIV-1 Tat in cardiomyocytes. *J. Cell. Physiol.* **2018**, *233*, 748–758. [[CrossRef](#)] [[PubMed](#)]
35. Brailoiu, E.; Deliu, E.; Sporic, R.A.; Benamar, K.; Brailoiu, G.C. HIV-1-Tat excites cardiac parasympathetic neurons of nucleus ambiguus and triggers prolonged bradycardia in conscious rats. *Am. J. Physiol. Integr. Comp. Physiol.* **2014**, *306*, R814–R822. [[CrossRef](#)]
36. Chen, Y.; Huang, W.; Jiang, W.; Wu, X.; Ye, B.; Zhou, X. HIV-1 Tat Regulates Occludin and A β Transfer Receptor Expression in Brain Endothelial Cells via Rho/ROCK Signaling Pathway. *Oxidative Med. Cell. Longev.* **2016**, *2016*, 4196572. [[CrossRef](#)]
37. Zou, M.; Huang, W.; Jiang, W.; Wu, Y.; Chen, Q. Role of Cav-1 in HIV-1 Tat-Induced Dysfunction of Tight Junctions and A β -Transferring Proteins. *Oxidative Med. Cell. Longev.* **2019**, *2019*, 3403206. [[CrossRef](#)]
38. Chen, Q.; Wu, Y.; Yu, Y.; Wei, J.; Huang, W. Rho-kinase inhibitor hydroxyfasudil protects against HIV-1 Tat-induced dysfunction of tight junction and neprilysin/A β transfer receptor expression in mouse brain microvessels. *Mol. Cell. Biochem.* **2021**, *476*, 2159–2170. [[CrossRef](#)]
39. Koyama, Y.; Takeishi, Y.; Niizeki, T.; Suzuki, S.; Kitahara, T.; Sasaki, T.; Kubota, I. Soluble Receptor for Advanced Glycation End Products (RAGE) is a Prognostic Factor for Heart Failure. *J. Card. Fail.* **2008**, *14*, 133–139. [[CrossRef](#)]
40. Ramasamy, R.; Schmidt, A.M. Receptor for Advanced Glycation End Products (RAGE) and Implications for the Pathophysiology of Heart Failure. *Curr. Heart Fail. Rep.* **2012**, *9*, 107–116. [[CrossRef](#)]
41. Hartog, J.W.L.; Voors, A.A.; Bakker, S.J.L.; Smit, A.J.; Van Veldhuisen, D.J. Advanced glycation end-products (AGEs) and heart failure: Pathophysiology and clinical implications. *Eur. J. Heart Fail.* **2007**, *9*, 1146–1155. [[CrossRef](#)] [[PubMed](#)]
42. Senatus, L.M.; Schmidt, A.M. The AGE-RAGE Axis: Implications for Age-Associated Arterial Diseases. *Front. Genet.* **2017**, *8*, 187. [[CrossRef](#)] [[PubMed](#)]
43. Zhou, Z.; Wang, K.; Penn, M.S.; Marso, S.P.; Lauer, M.A.; Forudi, F.; Zhou, X.; Qu, W.; Lu, Y.; Stern, D.M.; et al. Receptor for AGE (RAGE) Mediates Neointimal Formation in Response to Arterial Injury. *Circulation* **2003**, *107*, 2238–2243. [[CrossRef](#)]
44. Gao, X.; Zhang, H.; Schmidt, A.M.; Zhang, C. AGE/RAGE produces endothelial dysfunction in coronary arterioles in Type 2 diabetic mice. *Am. J. Physiol. Circ. Physiol.* **2008**, *295*, H491–H498. [[CrossRef](#)] [[PubMed](#)]
45. Wautier, M.-P.; Chappey, O.; Corda, S.; Stern, D.M.; Schmidt, A.M.; Wautier, J.-L. Activation of NADPH oxidase by AGE links oxidant stress to altered gene expression via RAGE. *Am. J. Physiol. Endocrinol. Metab.* **2001**, *280*, E685–E694. [[CrossRef](#)] [[PubMed](#)]
46. Burr, S.D.; Harmon, M.B.; Stewart, J.A., Jr. The Impact of Diabetic Conditions and AGE/RAGE Signaling on Cardiac Fibroblast Migration. *Front. Cell Dev. Biol.* **2020**, *8*, 112. [[CrossRef](#)]

47. El Kamari, V.; Thomas, A.; Shan, L.; Sattar, A.; Monnier, V.; Howell, S.K.; Beisswenger, P.J.; McComsey, G.A. Advanced Glycation End Products Are Associated with Inflammation and Endothelial Dysfunction in HIV. *JAIDS J. Acquir. Immune Defic. Syndr.* **2019**, *81*, e55–e62. [[CrossRef](#)]
48. El Kamari, V.; Rodriguez, K.; Moser, C.; Currier, J.S.; Kelesidis, T.; Stein, J.H.; Brown, T.T.; Howell, S.K.; Beisswenger, P.J.; AMccomsey, G. Advanced Glycation End Products Associated with Cardiometabolic Biomarkers In Treated HIV Infection. *Open Forum Infect. Dis.* **2021**, *8*, ofab423. [[CrossRef](#)]
49. Jeong, S.J.; Kim, C.O.; Song, Y.G.; Baek, J.-H.; Kim, S.B.; Jin, S.J.; Ku, N.S.; Han, S.H.; Choi, J.Y.; Lee, H.C.; et al. Low plasma levels of the soluble receptor for advanced glycation end products in HIV-infected patients with subclinical carotid atherosclerosis receiving combined antiretroviral therapy. *Atherosclerosis* **2011**, *219*, 778–783. [[CrossRef](#)]
50. Paris, J.J.; Zou, S.; Hahn, Y.K.; Knapp, P.E.; Hauser, K.F. 5 α -reduced progestogens ameliorate mood-related behavioral pathology, neurotoxicity, and microgliosis associated with exposure to HIV-1 Tat. *Brain Behav. Immun.* **2016**, *55*, 202–214. [[CrossRef](#)]
51. Bruce-Keller, A.J.; Turchan-Cholewo, J.; Smart, E.J.; Geurin, T.; Chauhan, A.; Reid, R.; Xu, R.; Nath, A.; Knapp, P.E.; Hauser, K.F. Morphine causes rapid increases in glial activation and neuronal injury in the striatum of inducible HIV-1 tat transgenic mice. *Glia* **2008**, *56*, 1414–1427. [[CrossRef](#)]
52. Eng, L.F.; Ghirnikar, R.S.; Lee, Y.L. Glial Fibrillary Acidic Protein: GFAP-Thirty-One Years (1969–2000). *Neurochem. Res.* **2000**, *25*, 1439–1451. [[CrossRef](#)]
53. Kashon, M.L.; Ross, G.W.; O’Callaghan, J.P.; Miller, D.B.; Petrovitch, H.; Burchfiel, C.M.; Sharp, D.S.; Markesbery, W.R.; Davis, D.G.; Hardman, J.; et al. Associations of cortical astrogliosis with cognitive performance and dementia status. *J. Alzheimers Dis.* **2004**, *6*, 595–604; discussion 673–681. [[CrossRef](#)]
54. Kikel-Coury, N.L.; Brandt, J.P.; Correia, I.A.; O’Dea, M.R.; DeSantis, D.F.; Sterling, F.; Vaughan, K.; Ozcebe, G.; Zorlutuna, P.; Smith, C.J. Identification of astroglia-like cardiac nexus glia that are critical regulators of cardiac development and function. *PLoS Biol.* **2021**, *19*, e3001444. [[CrossRef](#)]
55. Kawano, T.; Oki, T.; Uchida, T.; Iuchi, A.; Ogawa, S.; Hayashi, M.; Fukuda, N.; Mori, H.; Ii, K.; Hizawa, K. Innervation of the mitral valve in normal and prolapsed mitral valves. *J. Cardiol. Suppl.* **1989**, *21*, 43–54; discussion 55–56. (In Japanese) [[PubMed](#)]
56. Baldarelli, R.M.; Smith, C.M.; Finger, J.H.; Hayamizu, T.F.; McCright, I.J.; Xu, J.; Shaw, D.R.; Beal, J.S.; Blodgett, O.; Campbell, J.; et al. The mouse Gene Expression Database (GXD): 2021 update. *Nucleic Acids Res.* **2021**, *49*, D924–D931. [[CrossRef](#)]
57. Lucchetti, J.; Fracasso, C.; Balducci, C.; Passoni, A.; Forloni, G.; Salmona, M.; Gobbi, M. Plasma and Brain Concentrations of Doxycycline after Single and Repeated Doses in Wild-Type and APP23 Mice. *J. Pharmacol. Exp. Ther.* **2019**, *368*, 32–40. [[CrossRef](#)] [[PubMed](#)]
58. Lewis, W.; Grupp, I.L.; Grupp, G.; Hoit, B.; Morris, R.; Samarel, A.M.; Bruggeman, L.; Klotman, P. Cardiac dysfunction occurs in the HIV-1 transgenic mouse treated with zidovudine. *Lab. Invest.* **2000**, *80*, 187–197. [[CrossRef](#)] [[PubMed](#)]
59. Hoit, B.D.; Khoury, S.F.; Kranias, E.G.; Ball, N.; Walsh, R.A. In Vivo Echocardiographic Detection of Enhanced Left Ventricular Function in Gene-Targeted Mice with Phospholamban Deficiency. *Circ. Res.* **1995**, *77*, 632–637. [[CrossRef](#)] [[PubMed](#)]
60. Stewart, J.A.; Wei, C.-C.; Brower, G.L.; Rynders, P.E.; Hankes, G.H.; Dillon, A.R.; Lucchesi, P.A.; Janicki, J.S.; Dell’Italia, L.J. Cardiac mast cell- and chymase-mediated matrix metalloproteinase activity and left ventricular remodeling in mitral regurgitation in the dog. *J. Mol. Cell. Cardiol.* **2003**, *35*, 311–319. [[CrossRef](#)]
61. Erqou, S.; Lodebo, B.T.; Masri, A.; Altibi, A.M.; Echouffo-Tcheugui, J.B.; Dzudie, A.; Ataklte, F.; Choudhary, G.; Bloomfield, G.S.; Wu, W.-C.; et al. Cardiac Dysfunction Among People Living With HIV. *JACC Heart Fail.* **2019**, *7*, 98–108. [[CrossRef](#)]
62. Cerrato, E.; D’Ascenzo, F.; Biondi-Zoccai, G.; Calcagno, A.; Frea, S.; Marra, W.G.; Castagno, D.; Omedè, P.; Quadri, G.; Sciuto, F.; et al. Cardiac dysfunction in pauci symptomatic human immunodeficiency virus patients: A meta-analysis in the highly active antiretroviral therapy era. *Eur. Heart J.* **2013**, *34*, 1432–1436. [[CrossRef](#)] [[PubMed](#)]
63. Friis-Møller, N.; Weber, R.; Reiss, P.; Thiébaud, R.; Kirk, O.; d’Arminio Monforte, A.; Pradier, C.; Morfeldt, L.; Mateu, S.; Law, M.; et al. Cardiovascular disease risk factors in HIV patients—association with antiretroviral therapy. Results from the DAD study. *AIDS* **2003**, 1179–1193. [[CrossRef](#)]
64. Duprez, D.A.; Neuhaus, J.J.; Kuller, L.L.; Tracy, R.R.; Belloso, W.W.; De Wit, S.; Drummond, F.F.; Lane, H.C.H.; Ledergerber, B.; Lundgren, J.; et al. Inflammation, Coagulation and Cardiovascular Disease in HIV-Infected Individuals. *PLoS ONE* **2012**, *7*, e44454. [[CrossRef](#)]
65. Kuller, L.L.; Tracy, R.R.; Belloso, W.W.; De Wit, S.; Drummond, F.F.; Lane, C.H.; Ledergerber, B.; Lundgren, J.; Neuhaus, J.J.; Nixon, D.D.; et al. Inflammatory and Coagulation Biomarkers and Mortality in Patients with HIV Infection. *PLoS Med.* **2008**, *5*, e203. [[CrossRef](#)]
66. Green, L.A.; Kim, C.; Gupta, S.K.; Rajashekhar, G.; Rehman, J.; Clauss, M. Pentoxifylline reduces tumor necrosis factor- α and HIV-induced vascular endothelial activation. *AIDS Res. Hum. Retrovir.* **2012**, *10*, 1207–1215. [[CrossRef](#)] [[PubMed](#)]
67. Hsue, P.Y.; Waters, D.D. Time to Recognize HIV Infection as a Major Cardiovascular Risk Factor. *Circulation* **2018**, *138*, 1113–1115. [[CrossRef](#)]
68. Neumann, T.; Woiwod, T.; Neumann, A.; Miller, M.; Von Birgelen, C.; Volbracht, L.; Esser, S.; Brockmeyer, N.; Gerken, G.; Erbel, R. Cardiovascular risk factors and probability for cardiovascular events in HIV-infected patients-part III: Age differences. *Eur. J. Med. Res.* **2004**, *9*, 267–272.
69. Lai, L.; Qiu, H. The Physiological and Pathological Roles of Mitochondrial Calcium Uptake in Heart. *Int. J. Mol. Sci.* **2020**, *21*, 7689. [[CrossRef](#)] [[PubMed](#)]

70. Gustafsson, Å.B.; Gottlieb, R.A. Heart mitochondria: Gates of life and death. *Cardiovasc. Res.* **2008**, *77*, 334–343. [[CrossRef](#)] [[PubMed](#)]
71. Coughlan, M.T.; Thorburn, D.R.; Penfold, S.A.; Laskowski, A.; Harcourt, B.E.; Sourris, K.C.; Tan, A.L.; Fukami, K.; Thallas-Bonke, V.; Nawroth, P.P.; et al. RAGE-Induced Cytosolic ROS Promote Mitochondrial Superoxide Generation in Diabetes. *J. Am. Soc. Nephrol.* **2009**, *20*, 742–752. [[CrossRef](#)] [[PubMed](#)]
72. van Deel, E.D.; Lu, Z.; Xu, X.; Zhu, G.; Hu, X.; Oury, T.D.; Bache, R.J.; Duncker, D.J.; Chen, Y. Extracellular superoxide dismutase protects the heart against oxidative stress and hypertrophy after myocardial infarction. *Free Radic. Biol. Med.* **2008**, *44*, 1305–1313. [[CrossRef](#)]
73. Juul, K.; Tybjaerg-Hansen, A.; Marklund, S.; Heegaard, N.H.; Steffensen, R.; Sillesen, H.; Jensen, G.; Nordestgaard, B.G. Genetically Reduced Antioxidative Protection and Increased Ischemic Heart Disease Risk. *Circulation* **2004**, *109*, 59–65. [[CrossRef](#)] [[PubMed](#)]
74. Mondy, K.E.; Gottdiener, J.; Overton, E.T.; Henry, K.; Bush, T.; Conley, L.; Hammer, J.; Carpenter, C.C.; Kojic, E.; Patel, P.; et al. High Prevalence of Echocardiographic Abnormalities among HIV-infected Persons in the Era of Highly Active Antiretroviral Therapy. *Clin. Infect. Dis.* **2011**, *52*, 378–386. [[CrossRef](#)] [[PubMed](#)]
75. Hsue, P.Y.; Hunt, P.W.; Ho, J.E.; Farah, H.H.; Schnell, A.; Hoh, R.; Martin, J.N.; Deeks, S.G.; Bolger, A.F. Impact of HIV Infection on Diastolic Function and Left Ventricular Mass. *Circ. Heart Fail.* **2010**, *3*, 132–139. [[CrossRef](#)]
76. Schuster, I.; Thöni, G.J.; Ederhy, S.; Walther, G.; Nottin, S.; Vinet, A.; Boccard, F.; Khireddine, M.; Girard, P.-M.; Mauboussin, J.-M.; et al. Subclinical Cardiac Abnormalities in Human Immunodeficiency Virus-Infected Men Receiving Antiretroviral Therapy. *Am. J. Cardiol.* **2008**, *101*, 1213–1217. [[CrossRef](#)] [[PubMed](#)]
77. Redfield, M.M.; Jacobsen, S.J.; Burnett, J.C.; Mahoney, D.W.; Bailey, K.R.; Rodeheffer, R.J. Burden of Systolic and Diastolic Ventricular Dysfunction in the Community. *JAMA* **2003**, *289*, 194–202. [[CrossRef](#)]
78. Mansoor, A.; Golub, E.T.; Dehovitz, J.; Anastos, K.; Kaplan, R.C.; Lazar, J.M. The Association of HIV Infection with Left Ventricular Mass/Hypertrophy. *AIDS Res. Hum. Retrovir.* **2009**, *25*, 475–481. [[CrossRef](#)]
79. McIntosh, R.C. A meta-analysis of HIV and heart rate variability in the era of antiretroviral therapy. *Clin. Auton. Res.* **2016**, *26*, 287–294. [[CrossRef](#)]
80. Višković, K.; Židovec Lepej, S.; Gorenec, A.; Grgić, I.; Lukas, D.; Zekan, Š.; Dragobratović, A.; Trupković, M.; Begovac, J. Cardiovascular markers of inflammation and serum lipid levels in HIV-infected patients with undetectable viremia. *Sci. Rep.* **2018**, *8*, 6113–19548. [[CrossRef](#)]
81. Nou, E.; Lo, J.; Grinspoon, S.K. Inflammation, immune activation, and cardiovascular disease in HIV. *AIDS* **2016**, *30*, 1495–1509. [[CrossRef](#)] [[PubMed](#)]
82. Mooney, S.; Tracy, R.; Osler, T.; Grace, C. Elevated Biomarkers of Inflammation and Coagulation in Patients with HIV Are Associated with Higher Framingham and VACS Risk Index Scores. *PLoS ONE* **2015**, *10*, e0144312. [[CrossRef](#)] [[PubMed](#)]
83. Fang, Q.; Kan, H.; Lewis, W.; Chen, F.; Sharma, P.; Finkel, M.S. Dilated Cardiomyopathy in Transgenic Mice Expressing HIV Tat. *Cardiovasc. Toxicol.* **2009**, *9*, 39–45. [[CrossRef](#)] [[PubMed](#)]
84. McDonough, K.H.; Doumen, C.; Giaimo, M.; Prakash, O. Effects of the HIV-1 Protein Tat on Myocardial Function and Response to Endotoxin. *Cardiovasc. Toxicol.* **2010**, *10*, 250–258. [[CrossRef](#)]
85. Raidel, S.M.; Haase, C.; Jansen, N.R.; Russ, R.B.; Sutliff, R.L.; Velsor, L.W.; Day, B.J.; Hoit, B.D.; Samarel, A.M.; Lewis, W. Targeted myocardial transgenic expression of HIV Tat causes cardiomyopathy and mitochondrial damage. *Am. J. Physiol. Heart Circ. Physiol.* **2002**, *282*, H1672–H1678. [[CrossRef](#)]
86. Tahrir, F.G.; Knezevic, T.; Gupta, M.K.; Gordon, J.; Cheung, J.Y.; Feldman, A.M.; Khalili, K. Evidence for the Role of BAG3 in Mitochondrial Quality Control in Cardiomyocytes. *J. Cell. Physiol.* **2016**, *232*, 797–805. [[CrossRef](#)]
87. Parihar, P.; Parihar, M.S. Metabolic enzymes dysregulation in heart failure: The prospective therapy. *Heart Fail. Rev.* **2016**, *22*, 109–121. [[CrossRef](#)]
88. Fitting, S.; Knapp, P.E.; Zou, S.; Marks, W.; Bowers, M.S.; Akbarali, H.; Hauser, K.F. Interactive HIV-1 Tat and Morphine-Induced Synaptodendritic Injury Is Triggered through Focal Disruptions in Na⁺ Influx, Mitochondrial Instability, and Ca²⁺ Overload. *J. Neurosci.* **2014**, *34*, 12850–12864. [[CrossRef](#)]
89. Paris, J.J.; Liere, P.; Kim, S.; Mahdi, F.; Buchanan, M.E.; Nass, S.R.; Qrareya, A.N.; Salahuddin, M.F.; Pianos, A.; Fernandez, N.; et al. Pregnane steroidogenesis is altered by HIV-1 Tat and morphine: Physiological allopregnanolone is protective against neurotoxic and psychomotor effects. *Neurobiol. Stress* **2020**, *12*, 100211. [[CrossRef](#)]
90. Splawski, I.; Timothy, K.W.; Decher, N.; Kumar, P.; Sachse, F.B.; Beggs, A.H.; Sanguinetti, M.C.; Keating, M.T. Severe arrhythmia disorder caused by cardiac L-type calcium channel mutations. *Proc. Natl. Acad. Sci. USA* **2005**, *102*, 8089–8096; discussion 8086–8088. [[CrossRef](#)]
91. Koczor, C.A.; Fields, E.; Jedrzejczak, M.J.; Jiao, Z.; Ludaway, T.; Russ, R.; Shang, J.; Torres, R.A.; Lewis, W. Methamphetamine and HIV-Tat alter murine cardiac DNA methylation and gene expression. *Toxicol. Appl. Pharmacol.* **2015**, *288*, 409–419. [[CrossRef](#)] [[PubMed](#)]
92. Choi, J.; Liu, R.-M.; Kundu, R.K.; Sangiorgi, F.; Wu, W.; Maxson, R.; Forman, H.J. Molecular Mechanism of Decreased Glutathione Content in Human Immunodeficiency Virus Type 1 Tat-transgenic Mice. *J. Biol. Chem.* **2000**, *275*, 3693–3698. [[CrossRef](#)] [[PubMed](#)]
93. Song, H.Y.; Ju, S.M.; Lee, J.A.; Kwon, H.-J.; Eum, W.S.; Jang, S.H.; Choi, S.Y.; Park, J. Suppression of HIV-1 Tat-induced monocyte adhesiveness by a cell-permeable superoxide dismutase in astrocytes. *Exp. Mol. Med.* **2007**, *39*, 778–786. [[CrossRef](#)] [[PubMed](#)]

94. Flynn, J.M.; Melov, S. SOD2 in mitochondrial dysfunction and neurodegeneration. *Free Radic. Biol. Med.* **2013**, *62*, 4–12. [[CrossRef](#)] [[PubMed](#)]
95. Weisiger, R.A.; Fridovich, I. Mitochondrial superoxide simutase. Site of synthesis and intramitochondrial localization. *J. Biol. Chem.* **1973**, *13*, 4793–4796. [[CrossRef](#)]
96. Lebovitz, R.M.; Zhang, H.; Vogel, H.; Cartwright, J., Jr.; Dionne, L.; Lu, N.; Huang, S.; Matzuk, M.M. Neurodegeneration, myocardial injury, and perinatal death in mitochondrial superoxide dismutase-deficient mice. *Proc. Natl. Acad. Sci. USA* **1996**, *93*, 9782–9787. [[CrossRef](#)]
97. Marcus, D.L.; AStrafaci, J.; Freedman, M.L. Differential neuronal expression of manganese superoxide dismutase in Alzheimer’s disease. *Med. Sci. Monit.* **2006**, *12*, BR8–BR14.
98. Massaad, C.A.; Washington, T.M.; Pautler, R.G.; Klann, E. Overexpression of SOD-2 reduces hippocampal superoxide and prevents memory deficits in a mouse model of Alzheimer’s disease. *Proc. Natl. Acad. Sci. USA* **2009**, *106*, 13576–13581. [[CrossRef](#)]
99. Saha, R.N.; Pahan, K. Differential regulation of Mn-superoxide dismutase in neurons and astroglia by HIV-1 gp120: Implications for HIV-associated dementia. *Free Radic. Biol. Med.* **2007**, *42*, 1866–1878. [[CrossRef](#)]
100. Moon, T.C.; Befus, A.D.; Kulka, M. Mast Cell Mediators: Their Differential Release and the Secretory Pathways Involved. *Front. Immunol.* **2014**, *5*, 569. [[CrossRef](#)]
101. Luo, T.; Chen, B.; Zhao, Z.; He, N.; Zeng, Z.; Wu, B.; Fukushima, Y.; Dai, M.; Huang, Q.; Xu, D.; et al. Histamine H2 receptor activation exacerbates myocardial ischemia/reperfusion injury by disturbing mitochondrial and endothelial function. *Basic Res. Cardiol.* **2013**, *108*, 342. [[CrossRef](#)] [[PubMed](#)]
102. Zidar, D.A.; Juchnowski, S.; Ferrari, B.; Clagett, B.; Pilch-Cooper, H.A.; Rose, S.; Rodriguez, B.; McComsey, G.A.; Sieg, S.F.; Mehta, N.; et al. Oxidized LDL Levels Are Increased in HIV Infection and May Drive Monocyte Activation. *JAIDS J. Acquir. Immune Defic. Syndr.* **2015**, *69*, 154–160. [[CrossRef](#)] [[PubMed](#)]
103. Teer, E.; Essop, M.F. HIV and Cardiovascular Disease: Role of Immunometabolic Perturbations. *Physiology* **2018**, *33*, 74–82. [[CrossRef](#)] [[PubMed](#)]
104. Fukami, K.; Yamagishi, S.-I.; Okuda, S. Role of AGEs-RAGE System in Cardiovascular Disease. *Curr. Pharm. Des.* **2014**, *20*, 2395–2402. [[CrossRef](#)]
105. Fang, F.; Yu, Q.; Arancio, O.; Chen, D.; Gore, S.S.; Yan, S.S.; Yan, S.F. RAGE mediates A β accumulation in a mouse model of Alzheimer’s disease via modulation of β - and γ -secretase activity. *Hum. Mol. Genet.* **2018**, *27*, 1002–1014. [[CrossRef](#)]
106. Loeser, R.F.; Yammani, R.R.; Carlson, C.S.; Chen, H.; Cole, A.; Im, H.-J.; Bursch, L.S.; Du Yan, S. Articular chondrocytes express the receptor for advanced glycation end products: Potential role in osteoarthritis. *Arthritis Care Res.* **2005**, *52*, 2376–2385. [[CrossRef](#)]
107. Simm, A.; Caßelmann, C.; Schubert, A.; Hofmann, S.; Reimann, A.; Silber, R.-E. Age associated changes of AGE-receptor expression: RAGE upregulation is associated with human heart dysfunction. *Exp. Gerontol.* **2004**, *39*, 407–413. [[CrossRef](#)]
108. Grossin, N.; Auger, F.; Niquet-Leridon, C.; Durieux, N.; Montaigne, D.; Schmidt, A.M.; Susen, S.; Jacolot, P.; Beuscart, J.-B.; Tessier, F.J.; et al. Dietary CML-enriched protein induces functional arterial aging in a RAGE-dependent manner in mice. *Mol. Nutr. Food Res.* **2015**, *59*, 927–938. [[CrossRef](#)]
109. Mao, Y.X.; Cai, W.J.; Sun, X.Y.; Dai, P.P.; Li, X.M.; Wang, Q.; Huang, X.L.; He, B.; Wang, P.P.; Wu, G.; et al. RAGE-dependent mitochondria pathway: A novel target of silibinin against apoptosis of osteoblastic cells induced by advanced glycation end products. *Cell Death Dis.* **2018**, *9*, 674. [[CrossRef](#)]
110. Lo, M.-C.; Chen, M.-H.; Lee, W.-S.; Lu, C.-I.; Chang, C.-R.; Kao, S.-H.; Lee, H.-M. N^ε-(carboxymethyl) lysine-induced mitochondrial fission and mitophagy cause decreased insulin secretion from β -cells. *Am. J. Physiol. Metab.* **2015**, *309*, E829–E839. [[CrossRef](#)]
111. Teissier, T.; Boulanger, É. The receptor for advanced glycation end-products (RAGE) is an important pattern recognition receptor (PRR) for inflamming. *Biogerontology* **2019**, *20*, 279–301. [[CrossRef](#)] [[PubMed](#)]
112. Reddy, G.K. AGE-related cross-linking of collagen is associated with aortic wall matrix stiffness in the pathogenesis of drug-induced diabetes in rats. *Microvasc. Res.* **2004**, *68*, 132–142. [[CrossRef](#)] [[PubMed](#)]
113. Dickens, A.M.; Yoo, S.W.; Chin, A.C.; Xu, J.; Johnson, T.P.; Trout, A.L.; Hauser, K.F.; Haughey, N.J. Chronic low-level expression of HIV-1 Tat promotes a neurodegenerative phenotype with aging. *Sci. Rep.* **2017**, *7*, 7748. [[CrossRef](#)] [[PubMed](#)]